2022

Anisotropic magnetoexcitons in two-dimensional transition metal trichalcogenide semiconductors

Roman Ya. Kezerashvili
CUNY New York City Co

Anastasia Spiridonova
CUNY New York City College of Technology

Anisotropic magnetoexcitons in two-dimensional transition metal trichalcogenide semiconductors

Roman Ya. Kezerashvili and Anastasia Spiridonova
New York City College of Technology, City University of New York, Brooklyn, New York 11201, USA
and Graduate School and University Center, City University of New York, New York, New York 10016, USA

Direct and indirect excitons in Rydberg states in transition metal trichalcogenide (TMTC) monolayers, bilayers, and van der Waals (vdW) heterostructures in an external magnetic field are studied within the framework of the effective mass approximation. Binding energies of magnetoexcitons are calculated using the Rytova-Keldysh potential for direct magnetoexcitons and both the Rytova-Keldysh and Coulomb potentials for indirect magnetoexcitons. We report the magnetic field energy contribution to the binding energies and diamagnetic coefficients for magnetoexcitons that depend strongly on the effective mass anisotropy of electrons and holes. The comparative study of TMTCs and phosphorene is given. In TiS_3, $TiSe_3$, and $ZrSe_3$ the excitonic binding energies and diamagnetic coefficients demonstrate the same kind of anisotropy as in phosphorene. In contrast, ZrS_3 has the opposite anisotropy to phosphorene. The tunability of the binding energy of direct and indirect magnetoexcitons by the external magnetic field and the possibility to control the binding energy of magnetoexcitons in vdW heterostructures by manipulation of numbers of hBN monolayers are shown.

I. INTRODUCTION

In this millennium graphene has ignited tremendous research interest in two-dimensional (2D) layered materials. A stream of new 2D layered materials such as transition metal dichalcogenides (TMDCs), phosphorene, and Xenes (silicene, germanine, stanene) exhibit remarkable physical properties resulting from their crystal symmetry and reduced dimensionality. These materials exhibit a band gap, either direct or indirect, and in-plane structural isotropy. There exist a small number of materials with a strong in-plane structural anisotropy such as phosphorene, where a monolayer appears to be composed of two distinct planes made of puckered honeycomb structure, and 2D layered materials, namely, group-IVB transition metal trichalcogenides (TMTCs), that are a source of attraction in the last few years.

Layered TMTCs are a new class of anisotropic 2D materials composed of atomic layers bounded via weak van der Waals forces that exhibit quasi-one-dimensional behavior. This property stems from their unique highly anisotropic crystal structure where vastly different material properties can be attained from different crystal directions. The reduced symmetry in the crystal structure of the TMTCs sets them apart from graphene, TMDCs, and Xenes with their largely isotropic in-plane electrical and optical properties. Prototypical representatives of this new class of 2D materials are TiS_3,

ZrS_3, and $ZrSe_3$ that have been successfully synthesized and $TiSe_3$ which is a hypothetical compound. $TiSe_3$ exfoliation from the bulk crystal is theoretically predicted. The TiS_3 monolayer is the only TMTC which possesses a direct band gap. In contrast to TiS_3, $TiSe_3$, ZrS_3, and $ZrSe_3$ monolayers are all indirect gap semiconductors [1,2]. The chemical formula for TMTCs is generally given by MX_3, where M is a transition metal and X is a chalcogen. Monolayers MX_3 can be viewed as interconnected one-dimensional chains of triangular MX_3 prisms, with the M-X bonds in the chains being significantly shorter than those between the chains [1]. Crystal structures and typical mechanical, electrical, optical, magnetic, and charge density wave transport properties characterizing TMTCs are reviewed and discussed in reviews [3,4], and see references therein.

Over the course of six decades starting with pioneer works [5,6], excitons in semiconductors in a magnetic field have been studied. In Refs. [7–9] the authors presented the theoretical framework to investigate the physics of three-dimensional (3D) Mott-Wannier magnetoexcitons. Studies of excitonic states in an anisotropic 3D semiconductor and their behavior in a magnetic field were started a decade later [10,11]. Today the study of excitons in 2D materials in an external magnetic field is an active field of experimental and theoretical research. Direct magnetoexcitons in 2D materials such as TMDC and Xene monolayers are investigated in Refs. [12–18]. The Zeeman shift has been considered in Refs. [12,14,16,17,19–23], and the diamagnetic shift was addressed in Refs. [12–14,16–18,20,24–26]. For indirect excitons in double-layer heterostructures, Rydberg state binding energies are reported in [27–33], and the Zeeman shift is presented in Refs. [34–37].

Employing different theoretical approaches, excitons in anisotropic two-dimensional semiconducting crystals were investigated in Refs. [38–44] . The effect of anisotropy in the energy spectrum on the binding energy and structural properties of excitons in TMTCs was studied in Refs. [44–46]. Most recently, magnetoexcitons in phosphorene monolayers and van der Waals (vdW) heterostructures have been investigated in Ref. [47]. However, we still lack experimental and theoretical studies of the properties of excitons in TMTCs monolayers and heterostructures in an external magnetic field, when the magnetoexcitons are formed. The study of magnetoexcitons in TMTC materials may seem excessive after the study on magnetoexcitons in phosphorene [47]. However, phosphorene is not stable in air and toxic. That is why other materials with an anisotropy similar to or different from that of phosphorene but without phosphorene's disadvantages should be studied to understand their use in the device design.

In this paper we address this gap and study the effect of TMTC crystal anisotropy on the direct and indirect magnetoexciton binding energies and diamagnetic coefficients (DMCs) of Rydberg states $1s$, $2s$, $3s$, and $4s$ in the monolayer and heterostructure composed by two TMTC monolayers separated by a number of hexagonal boron nitride (hBN) monolayers. A Mott-Wannier model for 2D excitons in an external magnetic field is presented in Sec. II. We report the binding energies of excitons in freestanding (FS) and hBN-encapsulated TiS$_3$, TiSe$_3$, ZrS$_3$, and ZrSe$_3$ monolayers and the dependence of the contribution of an external magnetic field to the exciton binding energy on the magnetic field, and diamagnetic coefficients in TMTC monolayers and heterostructures in Sec. III. Conclusions follow in Sec. IV.

II. THEORETICAL MODEL

The experimental mapping of the band structure, computed electronic band structure and density of states of TMTC monolayers, and computed electron and hole effective masses at the conduction band minimum and valence band maximum leads to the conclusions for description of excitons within the effective mass approximation [1,48–52]. The use of a many-body perturbation theory by solving the Bethe-Salpeter equation (BSE) and a Wannier-Mott model for the excitons, that considers the anisotropic effective masses, indicates that the exciton binding energies found in the BSE step are in good agreement with those obtained in the framework of the effective mass approach [44]. The effective mass approach successfully was applied to study binding energies of excitons and trions in layered TMTC materials [42,44,45].

Consider a Mott-Wannier model for 2D excitons in an external magnetic field that takes into account the effective anisotropic masses and a screened Coulomb interaction. In the system under consideration, excitons are confined in a 2D FS and hBN-encapsulated TMTC monolayer, FS bilayer, and van der Waals (vdW) heterostructure with the interlayer distance D composed of the hBN layers. In the latter two cases, an equal number of electrons and holes reside in two opposite parallel TMTC monolayers. In contrast to TMDC, the anisotropic nature of the 2D TMTC semiconductor breaks the central symmetry. The asymmetry of the electron and hole dispersion in TMTC is reflected in the Schrödinger

equation for the Mott-Wannier magnetoexciton. Therefore, it is preferable to use Cartesian coordinates for the description of excitons. In the framework of the effective mass approximation, the Schrödinger equation for an interacting electron-hole pair with anisotropic masses in the external uniform and constant magnetic field $\mathbf{B} = (0, 0, B)$ in the TMTC monolayer can be found in [47]. The corresponding Schrödinger equation for the 2D exciton, after the separation of the center of mass of an electron-hole pair, $\mathbf{R}(X, Y)$, and the relative motion, $\mathbf{r}(x, y)$, can be written for excitonic Rydberg states as [8]

$$\left[-\frac{1}{2\mu_x}\frac{\partial^2}{\partial x^2} - \frac{1}{2\mu_y}\frac{\partial^2}{\partial y^2} + \frac{e^2}{8\mu_x}B^2x^2 + \frac{e^2}{8\mu_y}B^2y^2 \right.$$
$$\left. + V(x, y) \right] \Phi(x, y) = E\,\Phi(x, y), \qquad (1)$$

where $\mu_x = \frac{m_x^e m_x^h}{m_x^e + m_x^h}$ and $\mu_y = \frac{m_y^e m_y^h}{m_y^e + m_y^h}$ are the reduced masses, related to the relative motion of an electron-hole pair in the x and y directions, respectively; m_x^e, m_y^e and m_x^h, m_y^h are the electron and hole effective masses in the x and y directions, respectively, and the symmetric gauge is used. To get (1), following Gor'kov and Dzyaloshinskii [8], we used a canonical transformation to obtain the electron-hole pair relative motion wave function $\Phi(x, y)$. Equation (1) gives the binding energies, E_B, of magnetoexciton Rydberg states with zero center-of-mass momentum [8,53,54].

When the electron and hole are located in the 2D plane, due to nonlocal screening, one uses the Rytova-Keldysh (RK) potential [55,56] that is widely employed for the description of charge carriers' interaction in 2D materials. The RK potential is a central potential, and the interaction between the electron and hole in a monolayer has the following functional form,

$$V(r) = -\frac{\pi k e^2}{2\kappa\rho_0}\left[H_0\left(\frac{r}{\rho_0}\right) - Y_0\left(\frac{r}{\rho_0}\right) \right], \qquad (2)$$

where $r = r_e - r_h$ is the relative coordinate between the electron and hole. In Eq. (2) e is the charge of the electron, $\kappa = (\epsilon_1 + \epsilon_2)/2$ describes the surrounding dielectric environment, ϵ_1 and ϵ_2 are the dielectric constants below and above the monolayer, respectively, H_0 and Y_0 are the Struve and Bessel functions of the second kind, respectively, and ρ_0 is the screening length. The potential (2) has the same functional form as one derived in Ref. [57], where the macroscopic screening is quantified by the 2D polarizability. Following [57,58] the screening length ρ_0 can be written as $\rho_0 = 2\pi\chi_{2D}/\kappa$, where χ_{2D} is the 2D polarizability. 2D layer polarizability can be computed by standard first-principles technique [57] or considered as a phenomenological parameter.

Indirect magnetoexcitons formed by electrons and holes residing in two different TMTC monolayers in the bilayer or vdW heterostructure have a longer lifetime than the direct excitons due to longer recombination time. For indirect excitons, one can obtain the eigenfunctions and eigenenergies of

magnetoexcitons by solving Eq. (1) using the RK potential

$$V(\sqrt{\rho^2 + D^2}) = -\frac{\pi k e^2}{2\kappa \rho_0}\left[H_0\left(\frac{\sqrt{\rho^2 + D^2}}{\rho_0}\right)\right.$$
$$\left. - Y_0\left(\frac{\sqrt{\rho^2 + D^2}}{\rho_0}\right)\right] \quad (3)$$

or

$$V_C(\sqrt{\rho^2 + D^2}) = -\frac{k e^2}{\kappa(\sqrt{\rho^2 + D^2})} \quad (4)$$

when the electron and hole interact via the Coulomb potential. Equations (3) and (4), where $\rho^2 = x^2 + y^2$, describe the interaction between the electron and hole that are located in different parallel TMTC monolayers separated by a distance $D = h + N l_{\text{hBN}}$, where $l_{\text{hBN}} = 0.333$ nm is the thickness of the hBN layer and h is the TMTC monolayer thickness. Below for indirect magnetoexcitons, we report calculations for both the RK (2) and Coulomb (4) potentials. This aids in the understanding of the role of screening in TMTCs.

In TMTC materials, electron and hole bands have different anisotropies from each other: the anisotropic band structure of the conduction band is flatter in the p_x direction, whereas the valence band is flatter in the p_y direction. This is in sharp contrast to phosphorene in which both the conduction and the valence bands are flatter in the p_y direction. In phosphorene, charge carrier effective mass anisotropy with lighter effective masses along the armchair direction and heavier effective masses along the zigzag direction lead to the reduced mass anisotropy: $\mu_y > \mu_x$. For TMTCs we have a different picture: for TiS$_3$, TiSe$_3$, and ZrSe$_3$, $\mu_y > \mu_x$, while for ZrS$_3$, $\mu_x > \mu_y$. One can obtain from (1) the expectation value for the bound state energies:

$$E = \left\langle -\frac{1}{2\mu_x}\frac{\partial^2}{\partial x^2}\right\rangle + \left\langle -\frac{1}{2\mu_y}\frac{\partial^2}{\partial y^2}\right\rangle + \left\langle\frac{e^2}{8\mu_x}B^2 x^2\right\rangle$$
$$+ \left\langle\frac{e^2}{8\mu_y}B^2 y^2\right\rangle + \langle V(x,y)\rangle. \quad (5)$$

The terms in the latter expression could be viewed as the sum of the average values of the operators of kinetic, magnetic, and potential energies in 2D space obtained by using the corresponding eigenfunction $\Phi(x,y)$ of the magnetoexciton state. From Eq. (5) follows that when $\mu_x > \mu_y$ the contribution of the corresponding kinetic energy term is small that leads to larger binding energy but smaller contribution of the magnetic field. The relation $\mu_y > \mu_x$ leads to the opposite conclusion.

We studied the formation of magnetoexcitons in several two-dimensional materials: Xenes (silicene, germanene, and stanene) [18], transition metal dichalcogenides [25,26], and phosphorene [47]. The magnetoexcitons in these systems are described by the two-body Schrödinger equation which can be reduced to the one-dimensional radial equation for isotropic materials and two-dimensional equation for anisotropic materials such as phosphorene. For all these systems the contribution of the magnetic field is defined by the reduced mass of the electron-hole pair. The difference in description of these system is due to the difference of the total potential $W(x,y)$ that consists of two parts: two-dimensional electron-hole interaction and action of the magnetic field on

the electron-hole pair. The first part has the same analytical form for all 2D materials, and the strength is exclusively defined by the 2D materials' polarizability. The action of the magnetic field on the electron-hole system is inversely proportional to the effective reduced mass of the electron-hole pair and can depend on anisotropic properties of materials due to the effective mass anisotropy.

For Xenes and TMDCs, which are isotropic materials, a total potential is central: $W(x,y) = \frac{e^2}{8\mu_x}B^2 x^2 + \frac{e^2}{8\mu_y}B^2 y^2 + V(x,y) \equiv \frac{e^2}{8\mu}B^2 r^2 + V(r)$, where μ is the reduced mass of the electron-hole pair and $r = \sqrt{x^2 + y^2}$. For Xenes $m_e = m_h$ that leads to $\mu = m_{e(h)}$, and the contribution of magnetic field is proportional to the factor $1/m_{e(h)}$. For TMDCs the reduced mass μ of the electron-hole pair is always smaller than the smallest electron or hole effective mass $\mu < m_{e(h)}$. In contrast, for anisotropic materials such as phosphorene and TMTCs the contribution of the magnetic field depends on the reduced masses of the electron-hole pair in the x and y directions. Consequently, the electron and hole mass anisotropy leads to the anisotropy of the total potential. In Figs. 1(a) and 1(b) are shown the total potential comparison between the isotropic WSe$_2$ and anisotropic ZrSe$_3$ and both anisotropic phosphorene and ZrS$_3$, respectively. The analysis indicates that $W(x,y)$ for ZrSe$_3$ is stronger in the x direction and weaker in the y direction than one for WSe$_2$. For the anisotropic phosphorene and ZrS$_3$, $W(x,y)$ for ZrSe$_3$ is stronger in the y direction and weaker at short distances in the x direction. Such behavior distinguishes TMTC monolayers and phosphorene. The latter provides a novel insight into how the interaction with two different anisotropies in 2D systems leads to different magnetic field contributions to the binding energy of magnetoexcitons and marks the very first demonstration in the next section.

III. RESULTS OF CALCULATIONS AND DISCUSSION

Consider results of the study of binding energies, contribution of the magnetic field to the binding energies, and diamagnetic coefficients for monolayers and vdW heterostructures of TMTCs. In Figs. 1(c) and 1(d) are presented the magnetoexciton binding energies of Rydberg states 1s, 2s, 3s, and 4s in FS and hBN-encapsulated monolayers of different TMTCs. We solve Eq. (1) using the numerical approach [47] that successfully reproduces the results for the phosphorene binding energy. There are a few papers that give binding energies of excitons in TiS$_3$ monolayers [44,45]. To check the validity of the code, we have performed calculations for exciton binding energies with the parameters given in those papers and reproduced their results within 5%.

In our calculations for input parameters, we use electron and hole effective masses found in the literature and listed in Table I along with the corresponding reduced masses. For TiS$_3$ polarizability $\chi_{2D} = 7.057$ Å [45]. We did not find the polarizabilities for TiSe$_3$, ZrS$_3$, and ZrSe$_3$ computed by standard first-principles techniques in the literature. One can calculate a 2D polarizability as $\chi = h(\epsilon - 1)/4\pi$ [57], where ϵ is the dielectric constant of a bulk material and h is a monolayer thickness. Following [45] polarizabilities for these monolayers can be obtained using the dielectric constant of
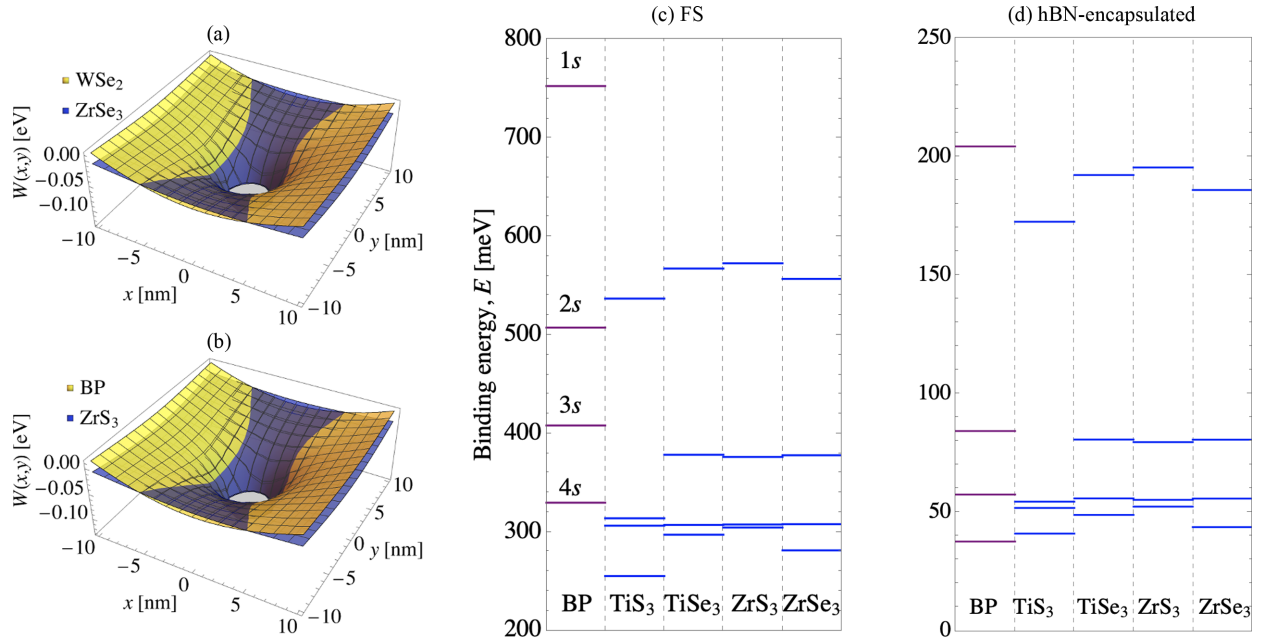
FIG. 1. Dependence of the total potential $W(x, y) = V(x, y) + \frac{e^2}{8\mu_x}B^2x^2 + \frac{e^2}{8\mu_y}B^2y^2$ acting on the electron-hole pair on x and y coordinates. Calculations are performed for the electron-hole pair in external magnetic field $B = 30$ T. (a) For WSe$_2$ with $\mu = 0.15m_0$ [59] and $\chi_{2D} = 7.571$ Å [60] and ZrSe$_3$ with $\mu_x = 0.15m_0$, $\mu_y = 0.79m_0$, and $\chi_{2D} = 9.322$ Å. (b) For ZrS$_3$ with $\mu_x = 0.64m_0$, $\mu_y = 0.2m_0$, and $\chi_{2D} = 7.057$ Å and phosphorene with $\mu_x = 0.063m_0$, $\mu_y = 0.97m_0$, and $\chi_{2D} = 4.1$ Å. The binding energies of excitons in phosphorene (BP: black phosphorus) and TMTC monolayers. (c) FS and (d) hBN-encapsulated. The calculations are performed using the anisotropic effective masses of electrons and holes from [61] for phosphorene and Refs. [1,45] for TMDC monolayers.

the material as a geometric average of its ϵ_x, ϵ_y, and ϵ_z components [63]. The thickness of the layers can be estimated from structural parameters given in Ref. [51].

For comparison in Figs. 1(c) and 1(d) are presented the corresponding binding energies for the phosphorene. The exciton binding energies in TMTCs do not vary significantly from substance to substance and are close enough. However, exciton binding energies of Rydberg states 1s, 2s, 3s, and 4s in TMTC monolayers are smaller than in phosphorene. Among TMTCs, ZrS$_3$ has the highest exciton binding energies of the 1s state in FS as well as the hBN-encapsulated monolayer. If one considers effective excitonic masses of the electron and hole for ZrS$_3$ from Ref. [62], where the ra-

tio $\mu_y/\mu_x = 0.32/1.26 = 0.26$ versus $\mu_y/\mu_x = 0.20/0.64 = 0.32$ from [1], the binding energies increase. For example, for the ZrS$_3$ FS monolayer, the increase is by about 14% and 21% for 1s and 2s, respectively, and ~23% for 3s and 4s states. The comparison of Figs. 1(c) and 1(d) shows that when TMTC materials are encapsulated in hBN the Rydberg state binding energies of the excitons are considerably smaller.

In Eq. (1), $W(x, y) = \frac{e^2}{8\mu_x}B^2x^2 + \frac{e^2}{8\mu_y}B^2y^2 + V(x, y)$ is a total potential that acts on the electron-hole system in the TMTC monolayer. Here the potential $V(x, y)$ has the central symmetry. The strength and particular behavior of the $V(x, y)$ potential is defined by the polarizability of 2D materials. The terms $\frac{e^2}{8\mu_x}B^2x^2$ and $\frac{e^2}{8\mu_y}B^2y^2$ present the anisotropic nature of $W(x, y)$. As a result of mass anisotropy, when $\mu_x > \mu_y$, $\frac{e^2}{8\mu_y}B^2y^2$ gives a larger contribution due to the magnetic field than the term $\frac{e^2}{8\mu_x}B^2x^2$ and vice versa if $\mu_y > \mu_x$. Thus, the electron and hole mass anisotropy leads to the anisotropy of $W(x, y)$. In Fig. 1(b), $W(x, y)$ is shown as a function of x and y for two anisotropic materials: ZrS$_3$ and phosphorene. The comparison demonstrates that while both potentials have anisotropy with respect to the x and y directions, phosphorene has deeper well and ZrS$_3$ exhibits more flat behavior. The same tendencies are observed when we consider ZrSe$_3$, TiSe$_3$, and TiSe$_3$ monolayers.

The dependence of magnetic field energy contribution to the exciton binding energy, ΔE, on the magnetic field for FS and hBN-encapsulated are presented in Fig. 2(a) and Fig. 2(b), respectively. We consider TiS$_3$ as the representative case. The results for TiSe$_3$, ZrS$_3$, and ZrSe$_3$ demonstrate the

TABLE I. The effective masses of the electron and hole in TMTC materials and corresponding reduced masses in the x and y directions. The masses are given in units of the free electron mass.

	Electron		Hole		Reduced mass	
	m_x^e	m_y^e	m_x^h	m_y^h	μ_x	μ_y
TiS$_3$	1.52[a]	0.40[a]	0.30[a]	0.99[a]	0.251	0.285
TiSe$_3$	0.19[b]	4.29[b]	3.57[b]	0.85[b]	0.180	0.709
ZrS$_3$	2.084[c]	0.624[c]	3.218[c]	0.682[c]	1.265	0.326
	1.3[b]	0.4[b]	1.28[b]	0.42[b]	0.645	0.205
ZrSe$_3$	0.16[b]	6.72[b]	2.36[b]	0.89[b]	0.150	0.786

[a]Reference [45].
[b]Reference [1].
[c]Reference [62].
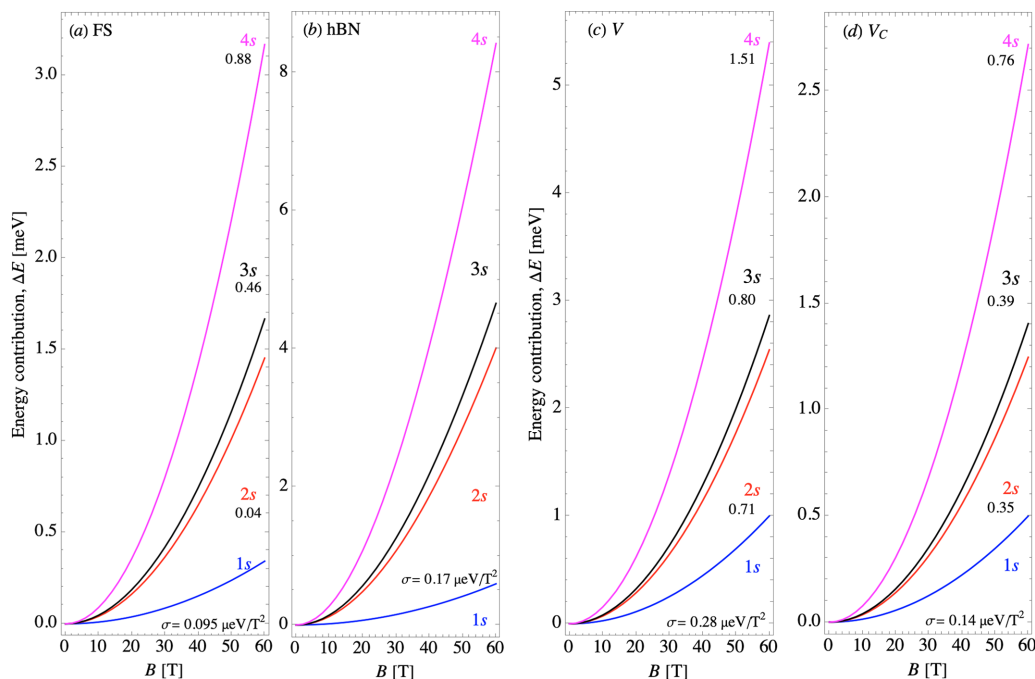
FIG. 2. The energy contribution of the magnetic field to the exciton binding energy as a function of the magnetic field in states $1s$, $2s$, $3s$, and $4s$ for TiS$_3$ monolayer and bilayer. (a) FS and (b) hBN-encapsulated monolayer. For TiS$_3$ bilayer calculations performed using both the Rytova-Keldysh and Coulomb potentials and presented in panels (c) and (d), respectively. On each graph we display the diamagnetic coefficients where they can be extracted. σ is given in μeV/T^2. DMCs are obtained for the range of the magnetic field between 0 and 30 T and correspond to $R^2 = 0.9998$ for the linear regression model.

same behavior with slightly different magnitudes. The linear dependence of ΔE on B^2 is observed in the range of magnetic field 0–30 T. So we use that range to extract the DMCs for states when the linear regime $\Delta E \sim B^2$ is valid. In FS TiS$_3$, DMCs can be extracted in all states and are listed in Fig. 2(a). The DMCs for $1s$, $2s$, $3s$, and $4s$ states increase from state to state and are significantly different. In hBN-encapsulated TiS$_3$ the DMC can be extracted only in the state $1s$ and is given in Fig. 2(b).

In Figs. 2(c) and 2(d) are presented the dependence of ΔE on the magnetic field for the TiS$_3$ bilayer. Calculations are performed for the Rytova-Keldysh (3) [Fig. 2(c)] and Coulomb (4) [Fig. 2(d)] potentials. In the same figures are listed corresponding DMCs. Interestingly enough, ΔE and DMCs calculated with the RK potential are twice as big as the magnetic energy contributions and DMCs for the Coulomb potential. Thus, the reduced dimensionality leads to an increase of the energy contributions of the magnetic field and DMCs for all Rydberg states.

We study the effect of anisotropy on the excitonic binding energy and energy contribution of the magnetic field to the binding energy of magnetoexcitons in TMTCs induced by the electron and hole masses anisotropy along the x and y directions. Analysis of Eqs. (1) and (5) shows the following: (i) a large μ_x leads to a sizable binding energy of excitons, because of the small contribution of kinetic energy; (ii) a large μ_y leads to a small contribution of the magnetic field to the binding energy of magnetoexcitons and vice versa. We study these phenomena in FS and hBN-encapsulated TiS$_3$, TiSe$_3$, and ZrSe$_3$ TMTC monolayers when different terms $1/\mu_x$ and $1/\mu_y$ are omitted in Eq. (1). In TiS$_3$, TiSe$_3$, and ZrSe$_3$

monolayers, the exciton binding energy in state $1s$ is dominated by the terms $1/\mu_y$. In contrast, in the FS and hBN-encapsulated ZrS$_3$ monolayer, the exciton binding energy in state $1s$ is dominated by the term proportional to $1/\mu_x$. These tendencies can be explained by the fact that in TiS$_3$, TiSe$_3$, and ZrSe$_3$ monolayers μ_y is bigger than μ_x, whereas in ZrS$_3$ the opposite picture is observed. Anisotropy similar to TiS$_3$, TiSe$_3$, and ZrSe$_3$ is observed in phosphorene where also $\mu_y > \mu_x$. It is worthwhile to emphasize that for FS TMTC monolayers, when we consider only the terms with $1/\mu_y$ in Eq. (1), the binding energy goes up by about 200–300 meV, while in the case of FS phosphorene, the binding energy doubles. In addition, in the case of FS TMTC, when we omit the terms proportional to $1/\mu_y$, again binding energies increase by about 200–300 meV.

The dominant contribution of the magnetic field to the binding energy of magnetoexcitons in TiS$_3$, TiSe$_3$, and ZrSe$_3$ comes from the term with $1/\mu_x$, while in ZrS$_3$ ΔE the dominant contribution comes from the term with $1/\mu_y$.

In Fig. 3, we compare ΔE and ΔE_C for the vdW heterostructure when two TiS$_3$ layers are separated by a number of hBN monolayers. Results are given for TiS$_3$, because it has been gaining interest due to its robust direct band gap, and it is taken to be the representative case. We plot ΔE as a function of the external magnetic field and the number of hBN layers. In vdW heterostructure formed by TiS$_3$ in the range of magnetic field between 0–30 T, the linear dependence of ΔE on B^2 is valid only for the $1s$ magnetoexciton, Fig. 3(a). DMCs can be extracted for the $1s$ state for the number of hBN layers up to $N = 3$ for magnetoexcitons with the Coulomb interaction, while for the RK potential one can extract the DMC in the
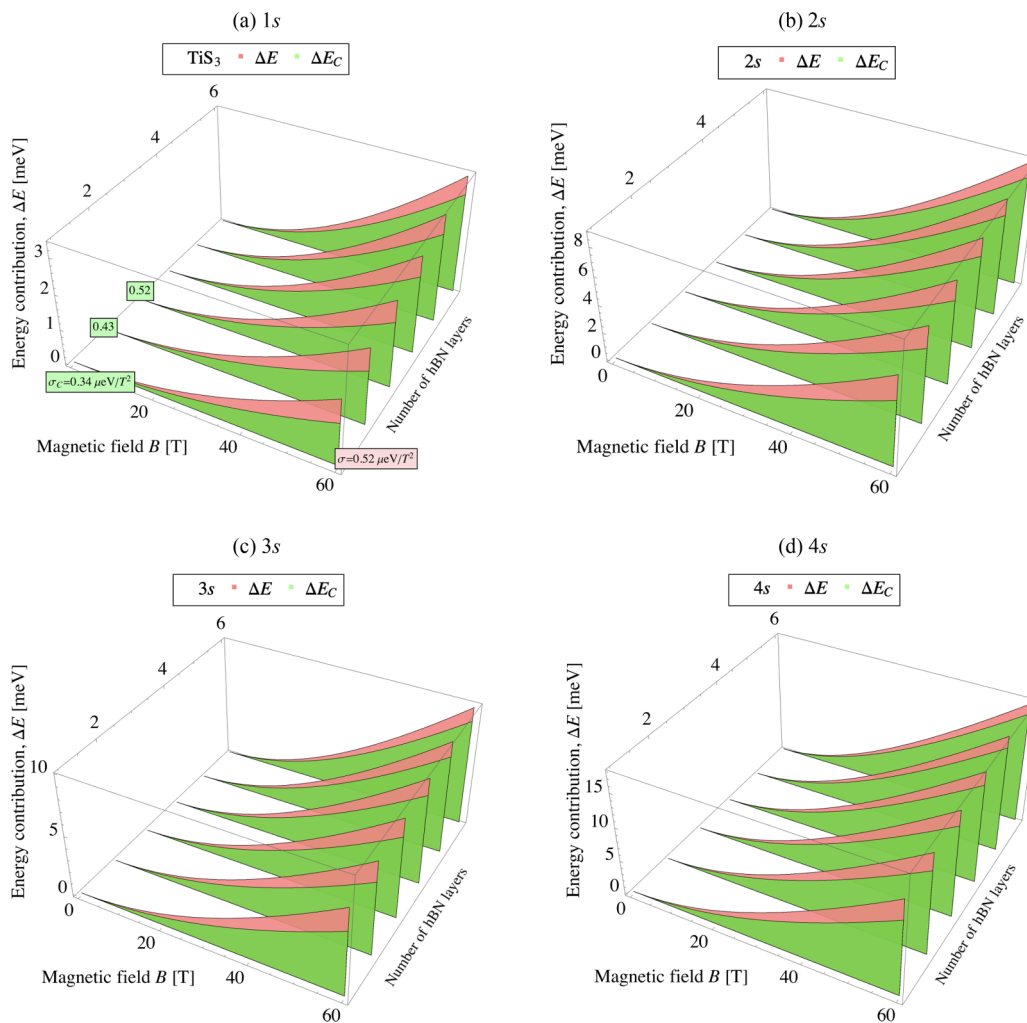
FIG. 3. The energy contribution of the magnetic field for indirect magnetoexcitons in the vdW heterostructures as a function of the magnetic field and the number of hBN layers. Calculations are performed for TiS$_3$ with input date from Ref. [45] using both the RK and Coulomb potentials. On the graph, we display the diamagnetic coefficients where they can be extracted. σ is given in μeV/T^2. DMCs are obtained for the range of the magnetic field between 0 and 30 T and correspond to $R^2 = 0.9998$ for the linear regression model.

state 1s only when $N = 1$. From Fig. 3 one can discern the following features: (i) in contrast to isotropic heterostructures built from TMDC monolayers, in TMTC vdW heterostructures indirect magnetoexcitons remain bound in all considered Rydberg states; (ii) $\Delta E > \Delta E_C$; (iii) as the number of hBN layers increases, ΔE and ΔE_C converge; (iv) the increase of both the magnetic field and the number hBN layers leads to an increase of the energy contribution of the magnetic field. In contrast to indirect magnetoexcitons in TMDC and Xene vdW heterostructures [18,26], ΔE due to the magnetic field in vdW TMTCs is always higher.

IV. CONCLUSIONS

In summary, we studied the binding energy and contribution of the magnetic field to the binding energy of direct and indirect magnetoexcitons in anisotropic 2D TMTC materials within the effective mass approximation. In our approach, exciton binding energy and DMCs are determined generally by the carrier effective mass anisotropy along the x and y directions and polarizability of 2D TMTC materials. For TMTC

materials the reduction of dimensionality from 3D to 2D leads to the increase of binding energies of excitons and DMCs due to the decrease of degree of freedom by unity and the screening of the electron-hole interaction. At the same time the electron and hole mass anisotropies allow excitons to be confined in a quasi-one-dimensional space [3,4] that leads to the additional increase of their binding energies and DMCs.

We found that magnetoexciton binding energy and ΔE are determined by the reduced masses of the electron and hole along the x and y directions. The mass anisotropy along the x and y directions causes the system to become quasi-one-dimensional that leads to the larger binding energies of excitons in TMTC materials, contrary to TMDCs. In TiS$_3$, TiSe$_3$, and ZrSe$_3$ the excitonic binding energies and DMCs demonstrate the same kind of anisotropy as in phosphorene. In contrast, ZrS$_3$ has the opposite anisotropy to phosphorene. In the absence of an external magnetic field, due to mass anisotropy, the term proportional to $1/\mu_y$ dominates the binding energy for TiS$_3$, TiSe$_3$, and ZrSe$_3$; this is in contrast to ZrS$_3$, where the main contribution is determined by the term proportional to $1/\mu_x$. For ΔE the picture is opposite: the

term proportional to $1/\mu_x$ gives the largest contribution for TiS$_3$, TiSe$_3$, and ZrSe$_3$, while for ZrS$_3$ the term with $1/\mu_y$ is dominant.

In bilayers and heterostructures, the electron and hole that interact through the $V(r)$ potential have a higher energy contribution than the ones interacting through V_C. In the range of the magnetic field 0–30 T, DMCs can be obtained for 1s, 2s, 3s, and 4s Rydberg states for FS and hBN-encapsulated TMTC monolayers, while for a vdW heterostructure only for the 1s state.

We demonstrated the tunability of the binding energy of direct and indirect magnetoexcitons by the external magnetic field and the possibility to control the binding energy of excitons in vdW heterostructures by manipulation of the number of hBN monolayers.

To the best of our knowledge, there are no experimental studies of magnetoexcitons in TMTC monolayers or their heterostructures. The magneto-optical spectroscopy at high magnetic field, which was recently used for the study magnetoexcitons in TMDC, provides an especially powerful way to identify and quantify excited Rydberg excitons because each excited state shifts very differently with magnetic field [12–14]. The excited states, being more loosely bound, are larger and, therefore, exhibit a significantly larger diamagnetic shift. Our calculations for the binding energies and DMCs of magnetoexcitons in TMTCs can provide the guideline for experimental studies.

Finally, it is worth mentioning that the advantage of phosphorene and TMTCs over TMDCs and Xenes is their anisotropic nature that can be used to create devices where different properties are needed along different directions. The advantage of TMTCs over phosphorene is that TMTCs are nontoxic, more abundant, and stable in air. In addition, as was shown, if TiS$_3$, TiSe$_3$, and ZrSe$_3$ possess anisotropy similar to phosphorene, ZrS$_3$ has anisotropy opposite to phosphorene that can be utilized in device design. It is already reported that TMTCs have possible applications as field effective transistors [64], solar and fuel devices [65–67], photodetectors and photosensors [68,69], lithium ion batteries [70], and in thermoelectricity [71], and devices that utilize anisotropy are on-chip polarizers [72,73], polarization-sensitive photodetectors [74], and devices with polarized light emissions [75].

[1] Y. Jin, X. Li, and J. Yang, Single layer of MX_3 (M = Ti, Zr; X = S, Se, Te): A new platform for nano-electronics and optics, Phys. Chem. Chem. Phys. **17**, 18665 (2015).

[2] M. Li, J. Dai, and X. C. Zeng, Tuning the electronic properties of transition-metal trichalcogenides via tensile strain, Nanoscale **7**, 15385 (2015).

[3] J. Dai, M. Li, and X. C. Zeng, Group IVB transition metal trichalcogenides: A new class of 2D layered materials beyond graphene, WIREs Comput. Mol. Sci. **6**, 211 (2016).

[4] A. Patra and C. Rout, Anisotropic quasi-one-dimensional layered transition-metal trichalcogenides: Synthesis, properties and applications, RSC Adv. **10**, 36413 (2020).

[5] R. Elliott and R. Loudon, Theory of the absorption edge in semiconductors in a high magnetic field, J. Phys. Chem. Solids **15**, 196 (1960).

[6] H. Hasegawa and R. Howard, Optical absorption spectrum of hydrogenic atoms in a strong magnetic field, J. Phys. Chem. Solids **21**, 179 (1961).

[7] M. Shinada and S. Sugano, Optical absorption edge in layer-type semiconductors, J. Phys. Soc. Jpn. **20**, 1274 (1965).

[8] L. P. Gorkov and I. E. Dzualoshinskii, Contribution to the theory of the Mott exciton in a strong magnetic field, Zh. Eksp. Teor. Fiz. **53**, 717 (1967) [JETP **26**, 449 (1968)].

[9] O. Akimoto and H. Hasegawa, Interband optical transitions in extremely anisotropic semiconductors. II. Coexistence of exciton and the Landau levels, J. Phys. Soc. Jpn. **22**, 181 (1967).

[10] M. Altarelli and N. O. Lipari, Perturbation-theory investigation of the exciton ground state of cubic semiconductors in a magnetic field, Phys. Rev. B **7**, 3798 (1973).

[11] L. Świerkowski, Direct excitons in cubic semiconductors in a magnetic field, Phys. Rev. B **10**, 3311 (1974).

[12] A. Stier, K. McCreary, B. Jonker, J. Kono, and S. Crooker, Exciton diamagnetic shifts and valley Zeeman effects in monolayer WS$_2$ and MoS$_2$ to 65 Tesla, Nat. Commun. **7**, 10643 (2016).

[13] J. Zipfel, J. Holler, A. A. Mitioglu, M. V. Ballottin, P. Nagler, A. V. Stier, T. Taniguchi, K. Watanabe, S. A. Crooker, P. C. M. Christianen, T. Korn, and A. Chernikov, Spatial extent of the excited exciton states in WS$_2$ monolayers from diamagnetic shifts, Phys. Rev. B **98**, 075438 (2018).

[14] A. V. Stier, N. P. Wilson, K. A. Velizhanin, J. Kono, X. Xu, and S. A. Crooker, Magnetooptics of Exciton Rydberg States in a Monolayer Semiconductor, Phys. Rev. Lett. **120**, 057405 (2018).

[15] M. N. Brunetti, O. L. Berman, and R. Ya. Kezerashvili, Optical properties of excitons in buckled two-dimensional materials in an external electric field, Phys. Rev. B **98**, 125406 (2018).

[16] E. Liu, J. van Baren, T. Taniguchi, K. Watanabe, Y.-C. Chang, and C. H. Lui, Magnetophotoluminescence of exciton Rydberg states in monolayer WS$_2$, Phys. Rev. B **99**, 205420 (2019).

[17] M. Goryca, J. Li, A. Stier, T. Taniguchi, K. Watanabe, E. Courtade, S. Shree, C. Robert, B. Urbaszek, X. Marie, and S. Crooker, Revealing exciton masses and dielectric properties of monolayer semiconductors with high magnetic fields, Nat. Commun. **10**, 4172 (2019).

[18] R. Ya. Kezerashvili and A. Spiridonova, Effects of parallel electric and magnetic fields on Rydberg excitons in buckled two-dimensional materials, Phys. Rev. B **103**, 165410 (2021).

[19] Y. Li, J. Ludwig, T. Low, A. Chernikov, X. Cui, G. Arefe, Y. D. Kim, A. M. van der Zande, A. Rigosi, H. M. Hill, S. H. Kim, J. Hone, Z. Li, D. Smirnov, and T. F. Heinz, Valley Splitting and Polarization by the Zeeman Effect in Monolayer MoSe$_2$, Phys. Rev. Lett. **113**, 266804 (2014).

[20] G. Plechinger, P. Nagler, A. Arora, A. Aguila, M. Ballottin, T. Frank, P. Steinleitner, M. Gmitra, J. Fabian, P. Christianen *et al.*, Excitonic valley effects in monolayer WS$_2$ under high magnetic fields, Nano Lett. **16**, 7899 (2016).

[21] D. V. Rybkovskiy, I. C. Gerber, and M. V. Durnev, Atomically inspired $k \cdot p$ approach and valley Zeeman effect in transition metal dichalcogenide monolayers, Phys. Rev. B **95**, 155406 (2017).

[22] M. Koperski, M. Molas, A. Arora, K. Nogajewski, M. Bartos, J. Wyzula, D. Vaclavkova, P. Kossacki, and M. Potemski, Orbital, spin and valley contributions to Zeeman splitting of excitonic resonances in MoSe$_2$, WSe$_2$ and WS$_2$ monolayers, 2D Mater. **6**, 015001 (2018).

[23] F. Xuan and S. Y. Quek, Valley Zeeman effect and Landau levels in two-dimensional transition metal dichalcogenides, Phys. Rev. Research **2**, 033256 (2020).

[24] M. Van der Donck, M. Zarenia, and F. M. Peeters, Excitons, trions, and biexcitons in transition-metal dichalcogenides: Magnetic-field dependence, Phys. Rev. B **97**, 195408 (2018).

[25] A. Spiridonova, Magnetoexcitons in monolayer transition-metal dichalcogenides, Phys. Lett. A **384**, 126850 (2020).

[26] R. Ya. Kezerashvili and A. Spiridonova, Magnetoexcitons in transition metal dichalcogenides monolayers, bilayers, and van der Waals heterostructures, Phys. Rev. Research **3**, 033078 (2021).

[27] J. He, K. Hummer, and C. Franchini, Stacking effects on the electronic and optical properties of bilayer transition metal dichalcogenides MoS$_2$, MoSe$_2$, WS$_2$, and WSe$_2$, Phys. Rev. B **89**, 075409 (2014).

[28] M. Palummo, M. Bernardi, and J. C. Grossman, Exciton radiative lifetimes in two-dimensional transition metal dichalcogenides, Nano Lett. **15**, 2794 (2015).

[29] I. C. Gerber and X. Marie, Dependence of band structure and exciton properties of encapsulated WSe$_2$ monolayers on the hBN-layer thickness, Phys. Rev. B **98**, 245126 (2018).

[30] M. Van der Donck and F. M. Peeters, Interlayer excitons in transition metal dichalcogenide heterostructures, Phys. Rev. B **98**, 115104 (2018).

[31] M. N. Brunetti, O. L. Berman, and R. Ya. Kezerashvili, Optical absorption by indirect excitons in a transition metal dichalcogenide/hexagonal boron nitride heterostructure, J. Phys.: Condens. Matter **30**, 225001 (2018).

[32] H. Kamban and T. Pedersen, Interlayer excitons in van der Waals heterostructures: Binding energy, Stark shift, and field-induced dissociation, Sci. Rep. **10**, 5537 (2020).

[33] E. V. Calman, L. H. Fowler-Gerace, D. J. Choksy, L. V. Butov, D. E. Nikonov, I. A. Young, S. Hu, A. Mishchenko, and A. K. Geim, Indirect excitons and trions in MoSe$_2$/WSe$_2$ van der Waals heterostructures, Nano Lett. **20**, 1869 (2020).

[34] A. Arora, M. Koperski, A. Slobodeniuk, K. Nogajewski, R. Schmidt, R. Schneider, M. R. Molas, S. M. de Vasconcellos, R. Bratschitsch, and M. Potemski, Zeeman spectroscopy of excitons and hybridization of electronic states in few-layer WSe$_2$, MoSe$_2$ and MoTe$_2$, 2D Mater. **6**, 015010 (2018).

[35] K. L. Seyler, P. Rivera, H. Yu, N. P. Wilson, E. L. Ray, D. G. Mandrus, J. Yan, W. Yao, and X. Xu, Signatures of moiré-trapped valley excitons in MoSe$_2$/WSe$_2$ heterobilayers, Nature (London) **567**, 66 (2019).

[36] T. Wang, S. Miao, Z. Li, Y. Meng, Z. Lu, Z. Lian, M. Blei, T. Taniguchi, K. Watanabe, S. Tongay, D. Smirnov, and S.-F. Shi,

Giant valley-Zeeman splitting from spin-singlet and spin-triplet interlayer excitons in WSe$_2$/MoSe$_2$ heterostructure, Nano Lett. **20**, 694 (2020).

[37] T. Woźniak, P. E. Faria Junior, G. Seifert, A. Chaves, and J. Kunstmann, Exciton *g* factors of van der Waals heterostructures from first-principles calculations, Phys. Rev. B **101**, 235408 (2020).

[38] A. Castellanos-Gomez, L. Vicarelli, E. Prada, J. O. Island, K. L. Narasimha-Acharya, S. I. Blanter, D. J. Groenendijk, M. Buscema, G. A. Steele, J. V. Alvarez *et al.*, Isolation and characterization of few-layer black phosphorus, 2D Mater. **1**, 025001 (2014).

[39] A. S. Rodin, A. Carvalho, and A. H. Castro Neto, Strain-Induced Gap Modification in Black Phosphorus, Phys. Rev. Lett. **112**, 176801 (2014).

[40] A. S. Rodin, A. Carvalho, and A. H. Castro Neto, Excitons in anisotropic two-dimensional semiconducting crystals, Phys. Rev. B **90**, 075429 (2014).

[41] E. Prada, J. V. Alvarez, K. L. Narasimha-Acharya, F. J. Bailen, and J. J. Palacios, Effective-mass theory for the anisotropic exciton in two-dimensional crystals: Application to phosphorene, Phys. Rev. B **91**, 245421 (2015).

[42] A. Chaves, M. Z. Mayers, F. M. Peeters, and D. R. Reichman, Theoretical investigation of electron-hole complexes in anisotropic two-dimensional materials, Phys. Rev. B **93**, 115314 (2016).

[43] O. L. Berman, G. Gumbs, and R. Ya. Kezerashvili, Bose-Einstein condensation and superfluidity of dipolar excitons in a phosphorene double layer, Phys. Rev. B **96**, 014505 (2017).

[44] E. Torun, H. Sahin, A. Chaves, L. Wirtz, and F. M. Peeters, *Ab initio* and semiempirical modeling of excitons and trions in monolayer TiS$_3$, Phys. Rev. B **98**, 075419 (2018).

[45] M. Van der Donck and F. M. Peeters, Excitonic complexes in anisotropic atomically thin two-dimensional materials: Black phosphorus and TiS$_3$, Phys. Rev. B **98**, 235401 (2018).

[46] Z. Jiang, Y. Li, S. Zhang, and W. Duan, Realizing an intrinsic excitonic insulator by decoupling exciton binding energy from the minimum band gap, Phys. Rev. B **98**, 081408(R) (2018).

[47] R. Ya. Kezerashvili, A. Spiridonova, and A. Dublin, Magnetoexcitons in phosphorene monolayers, bilayers, and van der Waals heterostructures, Phys. Rev. Research **4**, 013154 (2022).

[48] H. Yi, T. Komesu, S. Gilbert, G. Hao, A. J. Yost, A. Lipatov, A. Sinitskii, J. Avila, C. Chen, M. C. Asensio, and P. A. Dowben, The band structure of the quasi-one-dimensional layered semiconductor TiS$_3$(001), Appl. Phys. Lett. **112**, 052102 (2018).

[49] A. Pant, E. Torun, B. Chen, S. Bhat, X. Fan, K. Wu, D. P. Wright, F. M. Peeters, E. Soignard, H. Sahin, and S. Tongay, Strong dichroic emission in the pseudo one dimensional material ZrS$_3$, Nanoscale **8**, 16259 (2016).

[50] J. A. Silva-Guillén, E. Canadell, P. Ordejón, F. Guinea, and R. Roldán, Anisotropic features in the electronic structure of the two-dimensional transition metal trichalcogenide TiS$_3$: Electron doping and plasmons, 2D Mater. **4**, 025085 (2017).

[51] Y. Saeed, A. Kachmar, and M. A. Carignano, First-principles study of the transport properties in bulk and monolayer MX_3 (M = Ti, Zr, Hf and X = S, Se) compounds, J. Phys. Chem. C **121**, 1399 (2017).

[52] J. O. Island, A. J. Molina-Mendoza, M. Barawi, R. Biele, E. Flores, J. M. Clamagirand, J. R. Ares, C. Sánchez, H. S. J. van

der Zant, R. D'Agosta, I. J. Ferrer, and A. Castellanos-Gomez, Electronics and optoelectronics of quasi-1D layered transition metal trichalcogenides, 2D Mater. **4**, 022003 (2017).

[53] A. H. MacDonald and D. S. Ritchie, Hydrogenic energy levels in two dimensions at arbitrary magnetic fields, Phys. Rev. B **33**, 8336 (1986).

[54] Y. Lozovik and A. Ruvinsky, Magnetoexcitons in coupled quantum wells, Phys. Lett. A **227**, 271 (1997).

[55] N. Rytova, Screened potential of a point charge in a thin film, Proc. Moscow State University, Phys. Astron. **3**, 30 (1967).

[56] L. V. Keldysh, Coulomb interaction in thin semiconductor and semimetal films, JETP Lett. **29**, 658 (1979).

[57] P. Cudazzo, I. V. Tokatly, and A. Rubio, Dielectric screening in two-dimensional insulators: Implications for excitonic and impurity states in graphane, Phys. Rev. B **84**, 085406 (2011).

[58] T. C. Berkelbach, M. S. Hybertsen, and D. R. Reichman, Theory of neutral and charged excitons in monolayer transition metal dichalcogenides, Phys. Rev. B **88**, 045318 (2013).

[59] A. Kormányos, G. Burkard, M. Gmitra, J. Fabian, V. Zólyomi, N. D. Drummond, and V. Fal'ko, $k \cdot p$ theory for two-dimensional transition metal dichalcogenide semiconductors, 2D Mater. **2**, 022001 (2015).

[60] I. Kylänpää and H.-P. Komsa, Binding energies of exciton complexes in transition metal dichalcogenide monolayers and effect of dielectric environment, Phys. Rev. B **92**, 205418 (2015).

[61] C. J. Páez, K. DeLello, D. Le, A. L. C. Pereira, and E. R. Mucciolo, Disorder effect on the anisotropic resistivity of phosphorene determined by a tight-binding model, Phys. Rev. B **94**, 165419 (2016).

[62] C. Wang, C. Zheng, and G. Gao, Bulk and monolayer ZrS$_3$ as promising anisotropic thermoelectric materials: A comparative study, J. Phys. Chem. C **124**, 6536 (2020).

[63] L. D. Landau and E. M. Lifshitz, *Electrodynamics of Continuous Media*, 2nd ed. (Pergamon, Amsterdam, 1984).

[64] A. Lipatov, P. M. Wilson, M. Shekhirev, J. D. Teeter, R. Netusil, and A. Sinitskii, Few-layered titanium trisulfide (TiS$_3$) field-effect transistors, Nanoscale **7**, 12291 (2015).

[65] M. Barawi, E. Flores, I. J. Ferrer, J. R. Ares, and C. Sánchez, Titanium trisulphide (TiS$_3$) nanoribbons for easy hydrogen photogeneration under visible light, J. Mater. Chem. A **3**, 7959 (2015).

[66] R. Ahammed, A. Rawat, N. Jena, Dimple, M. K. Mohanta, and A. D. Sarkar, ZrS$_3$/MS$_2$ and ZrS$_3$/*MXY* type-II van der Waals hetero-bilayers: Prospective candidates in 2D excitonic solar cells, Appl. Surf. Sci. **499**, 143894 (2020).

[67] G. Shirota, A. Nasu, M. Deguchi, A. Sakuda, M. Tatsumisago, and A. Hayashi, Electrode performance of amorphous MoS$_3$ in all-solid-state sodium secondary batteries, J. Power Sources **10**, 100061 (2021).

[68] Q. Zhao, Y. Guo, Y. Zhou, Z. Yao, Z. Ren, J. Bai, and X. Xu, Band alignments and heterostructures of monolayer transition metal trichalcogenides MX_3 (M = Zr, Hf; X = S, Se) and dichalcogenides MX_2 (M = Tc, Re; X = S, Se) for solar applications, Nanoscale **10**, 3547 (2018).

[69] W. Wu, Y. Wang, Y. Niu, P. Wang, M. Chen, J. Sun, N. Wang, D. Wu, and Z. Zhao, Thermal localization enhanced fast photothermoelectric response in a quasi-one-dimensional flexible NbS$_3$ photodetector, ACS Appl. Mater. Interfaces **12**, 14165 (2020).

[70] J. Wu, D. Wang, H. Liu, W.-M. Lau, and L.-M. Liu, An ab initio study of TiS$_3$: A promising electrode material for rechargeable Li and Na ion batteries, RSC Adv. **5**, 21455 (2015).

[71] K. Biswas, J. He, I. D. Blum, C.-I. Wu, T. P. Hogan, D. N. Seidman, V. P. Dravid, and M. G. Kanatzidis, High-performance bulk thermoelectrics with all-scale hierarchical architectures, Nature (London) **489**, 414 (2012).

[72] M. Guillaumée, L. A. Dunbar, C. Santschi, E. Grenet, R. Eckert, O. J. F. Martin, and R. P. Stanley, Polarization sensitive silicon photodiodes using nanostructured metallic grids, Appl. Phys. Lett. **94**, 193503 (2009).

[73] S. Shishido, T. Noda, K. Sasagawa, T. Tokuda, and J. Ohta, Polarization analyzing image sensor with on-chip metal wire grid polarizer in 65-nm standard complementary metal oxide semiconductor process, Jpn. J. Appl. Phys. **50**, 04DL01 (2011).

[74] H. Yuan, X. Liu, F. Afshinmanesh, W. Li, G. Xu, J. Sun, B. Lian, A. G. Curto, G. Ye, Y. Hikita, Z. Shen, S.-C. Zhang, X. Chen, M. Brongersma, H. Y. Hwang, and Y. Cui, Polarization-sensitive broadband photodetector using a black phosphorus vertical p-n junction, Nat. Nanotechnol. **10**, 707 (2015).

[75] S. B. Singer, M. Mecklenburg, E. R. White, and B. C. Regan, Polarized light emission from individual incandescent carbon nanotubes, Phys. Rev. B **83**, 233404 (2011).